Surface-thermal capacity of D_2O from measurements made during steady-state evaporation

Fei Duan and C. A. Ward
Thermodynamics and Kinetics Laboratory, Department of Mechanical and Industrial Engineering, University of Toronto, 5 King's College Road, Toronto, Ontario, Canada M5S 3G8
(Received 26 November 2004; published 2 November 2005)

When $D_2O(l)$ evaporates into its vapor under steady-state conditions with the temperature field in the liquid arranged so that there is no buoyancy-driven convection and the Marangoni number is less than ~100, it is found that the interface is quiescent and thermal conduction to the interface supplies energy at a sufficient rate to evaporate the liquid. However, if the evaporation rate is raised so that the Marangoni number goes above ~100, the interface is transformed: a fluctuating thermocapillary flow occurs, and thermal conduction no longer supplies energy at a sufficient rate to evaporate the liquid. An energy analysis indicates conservation of energy can be satisfied only if thermocapillary convection is taken into account, and the surface-thermal capacity c_σ is assigned a value of 32.5 ± 0.8 kJ/(m^2 K) when the temperature is in the range $-10\ ^\circ\mathrm{C} \leqslant T^{LV} \leqslant 3.7\ ^\circ\mathrm{C}$. This value is consistent with that found previously for H_2O, and application of the Gibbs model gives a qualitative explanation for the value. Once the value of the surface-thermal capacity is known, the local heat flux along the interface can be calculated and statistical rate theory can be used to predict the local vapor-phase pressure on the interface. Since this theory introduces no adjustable parameters, the predicted pressure can be compared directly with that measured: this comparison indicates the mean of the pressures predicted to exist on the interface is in close agreement with those measured ~20 cm above the interface, and the small pressure gradient along the interface is consistent with the thermocapillary convection predicted from the interfacial temperature gradient.

DOI: 10.1103/PhysRevE.72.056304 PACS number(s): 47.20.Dr

I. INTRODUCTION

Measurements have been reported of the conditions at the interface of water as it evaporates into its own vapor, under steady-state conditions, while maintained at either the circular mouth of a stainless-steel funnel [1,2] or at the rectangular mouth of a V-shaped, stainless-steel channel [3,4]. In the former case, the liquid-vapor interface was spherical and in the latter cylindrical. The conditions at the interface when the liquid was evaporating at different rates were explored by reducing the pressure in the vapor phase to different values and increasing the water pumping rate in corresponding steps so as to maintain the liquid-vapor interface at approximately the same height above the funnel or channel mouth, while maintaining the temperature at the entry to either the funnel or the channel essentially constant at a temperature less than 4 °C. Evaporation cooled the liquid-vapor interface below that of the entry. Since water has it maximum density at 4 °C and since water density decreases monotonically as the temperature is decreased below 4 °C, there was no buoyancy-driven convection in either configuration. This means the roll-type convection normally associated with Marangoni-Bénard convection [5] was not present in these experiments. Thermal conduction transported energy from the entry of the funnel or channel to the rim of each. This raised the interfacial liquid temperature at the rim above that at the central axis of the spherical interface and above that on the longitudinal, central axis of the cylindrical interface. As the evaporation rate was raised, the Marangoni number (Ma) [6] was increased [see Eq. (1) below].

For the spherical interface, if Ma was less than ~100, the interface region was quiescent and thermal conduction in the liquid and vapor phases provided the energy required to evaporate the liquid at the observed rate [2]. However, when $100 < \mathrm{Ma} < 22{,}000$ thermocapillary convection was present and thermal conduction through the liquid and vapor phases no longer provided sufficient energy to evaporate the liquid. In a series of experiments, at progressively higher evaporation rates, the thermal conduction through the fluid phases accounted for a progressively *smaller* portion of the energy transport, reducing to ~60% as Ma approached 22,000. It was suggested that the additional energy was transported by thermal conduction from the thermostated entry to the funnel through the funnel walls to the rim where the liquid at the interface was heated. The measured interfacial liquid temperature profile at the spherical interface was axisymmetric and parabolic with the minimum on the center line and maximum at the rim. This temperature profile gave rise to thermocapillary convection [1], and this convection transported energy from the funnel rim along the interface.

In order to take the energy transport by thermocapillary convection into account quantitatively, it was necessary to introduce a new interfacial property of water: the surface-thermal capacity c_σ [2]. An equation relating c_σ to measurable quantities was obtained by applying the Gibbs dividing-surface approximation [7], the principles of molecular and energy conservation, and an expression for the thermocapillary speed ν_θ^{LV}, which had been previously introduced and examined experimentally [1]. All of the parameters appearing in the equation for c_σ could be determined by measuring the temperature fields in each phase. The value of c_σ was first determined from the data obtained in nine experiments at the spherical liquid-vapor interface in which $100 < \mathrm{Ma} < 22{,}000$, the average evaporation flux and interfacial temperature were in the range $0.10 < \overline{j_{ev}} < 3.38 \times 10^{-3}$ kg/(m^2 s) and $-10 < T^{LV} < 3.5\ ^\circ\mathrm{C}$. The surface-thermal capacity was found to

have a value of 30.6 ± 0.8 kJ/(m^2 K) in each experiment, and when the energy transport rate to the interface by thermocapillary convection was added to that by thermal conduction, the energy conservation principle was satisfied in each of the nine experiments [2]. These results suggest that c_σ is a property of water.

Nonetheless, the volumetric specific heat of bulk water at 0 °C is 4.23×10^3 kJ/(m^3 K). So the inferred value of c_σ appears larger than would be expected, at least for an equilibrium interface. To determine if c_σ should be viewed as a property of water or as an *ad hoc* quantity, a series of experiments with water evaporating from a cylindrical interface was performed [3]. The areas of the cylindrical water-vapor interfaces in these experiments were, on average, 4.4 times larger than in those experiments in which the interfaces were spherical. Buoyancy-driven convection was again eliminated, but thermocapillary convection was present. Thermal conduction accounted for as little as 50% of the energy required to evaporate the liquid in this case as well. The value of c_σ inferred from measurements made with water evaporating at the spherical interface was used to *predict* the energy transport by thermocapillary convection, and when this energy transport was added to that by thermal conduction, it was found that the conservation of energy principle was completely satisfied. The calculated and measured energy flux to the interface did not differ by more than ±2.5%. Thus the increased interfacial area did not reveal any error in the previously determined value of c_σ.

A second assessment of the surface-thermal capacity was conducted. In each experiment with water evaporating from a cylindrical interface, the c_σ value was used with the measured temperature profiles in the liquid and vapor phases to calculate the local evaporation flux j_{ev} along the interface from the measured temperature profiles. Then statistical rate theory [8–20] was applied to calculate the local vapor-phase pressures along the interface from the values of j_{ev}. No adjustable parameters are introduced by statistical rate theory; thus, the calculated pressure may be compared directly with the measured values. The mean of the calculated vapor-phase pressures on the interface was found to agree well with the vapor-phase pressure measured ~10 cm above the interface, and the predicted small gradient in pressure along the interface was consistent with the thermocapillary-generated flow [3].

These results confirm those obtained at the spherical interface and appear to support interpreting c_σ as an interfacial property of water when thermocapillary convection is active. The mechanism by which c_σ could have its inferred value has not been established, but it should be recalled that its value has been determined on the basis of the Gibbs model of the interface [7]. The present molecular models of water suggests that water may be viewed, for many purposes, as a hydrogen-bonded network with the water molecules vibrating-about their quasiequilibrium positions [21–23]. A study of thermocapillary-generated flow with a 12.7-μm-diam cylindrical probe with one end cantilever mounted and the other inserted a small distance into the interface of water as it evaporated under steady-state conditions indicated that the flow is always in the direction of increasing surface tension, but the flow is unsteady in magnitude [1]. If the surface molecules of the hydrogen-bonded network are being pulled in one direction, one could reasonably expect the hydrogen bonds to be stretched and the effect of the surface to extend deeper into the liquid phase than would be the case if equilibrium existed at the liquid-vapor interface. The Gibbs model of the system assigns this energy to the surface phase [2,3,7]. For H_2O the ratio of the surface-thermal capacity c_σ to the volumetric specific heat c_v is 7.2 ± 0.2 mm. The magnitude of the ratio indicates the strength of the interactions at the interface when thermocapillary convection is present. These interactions include the surface tension itself and the energy transported by the thermocapillary convection. The latter reached 50% of the energy required to evaporate the liquid at the observed rate for the cylindrical interface and 40% for the spherical interface [1–3]; however, c_σ is a model quantity and c_σ/c_v does not indicate the "depth" to which the bulk liquid is affected by the surface phase. The question arises of whether the Gibbs model of the surface phase would give a consistent description of the energy transport by thermocapillary convection and of whether it is the hydrogen-bonded network of water that is responsible for the transport of so much energy by thermocapillary convection. If it is the hydrogen-bonded network of water that plays a central role, then similar values of c_σ should be found for another hydrogen-bonded liquid, D_2O.

To examine this possibility, the value of c_σ for D_2O has been measured under conditions that are similar to the conditions that existed during the water evaporation experiments: D_2O liquid was maintained at the circular mouth of the same funnel as that used in the H_2O experiments, and the temperature at the funnel throat was again maintained at a temperature ~3.65 °C as D_2O evaporated steadily, but at different rates. Since the maximum density of D_2O occurs at 11.185 °C (see the Appendix), this ensures no buoyancy-driven convection was present in these experiments either.

II. EXPERIMENTAL APPARATUS AND PROCEDURE

The apparatus used was the same as that used to examine the conditions at the interface of water with its vapor during steady-state evaporation [1]. Briefly, $D_2O(\ell)$ with a minimum isotopic purity of 99.92% atomic D was transferred into a glass vessel, where it was degassed for 12 h while being stirred. A sample was taken for surface tension measurement, and the result was found to agree with the documented value at the same temperature to within 1%. The degassed $D_2O(\ell)$ could be transferred from the glass container by a stainless-steel tube into a glass syringe without exposure to air. The syringe pump plunger was advanced to push the degassed $D_2O(\ell)$ into the throat of a vertically oriented, stainless-steel funnel and on to the funnel mouth (7 mm diameter). The conical funnel (3.39 mm deep, with an included angle of 82°) was enclosed in a stainless-steel and glass vacuum chamber and could be viewed from outside the chamber with two cathetometers at viewing angles separated by 90°. The chamber was connected to two evacuating facilities: a turbo-molecular and associated backing pump and a separate mechanical vacuum pump.

Before an experiment, the vacuum chamber and syringe pump were evacuated to a pressure of $\sim 10^{-5}$ Pa during a ~12-h period. The degassed $D_2O(\ell)$ was then introduced into the syringe, without exposure to air, and pumped to the funnel mouth by advancing the syringe pump. To prevent subsequent bubble formation, with the $D_2O(\ell)$ at the funnel mouth, the chamber was pressurized with nitrogen to ~42 kPa for ~6 h. Afterwards, the pressure in the chamber was released, and ~2.0 ml of $D_2O(\ell)$ was flushed out through the funnel and into the chamber. The chamber was then evacuated with a separate mechanical vacuum pump until dry. The syringe pump was advanced again to bring the $D_2O(l)$-vapor interface to a maximum height of ~1 mm above the mouth of the funnel. During each experiment, the temperature of the $D_2O(\ell)$ at the funnel throat was monitored with a thermocouple fixed at that position and was maintained at ~3.65 °C with a thermostated circulator. This is below the temperature at which $D_2O(\ell)$ has its maximum density (11.185 °C; see the Appendix). The temperature at the interface in each phase was found to be less than 3.65 °C. Since the liquid phase expands on cooling for temperatures below 11.185 °C, there was no buoyancy-driven convection in the liquid phase.

When the liquid-vapor interface had been positioned so that its maximum height was ~1 mm above the funnel rim and the $D_2O(\ell)$ in the funnel throat was at ~3.65 °C, an experiment was initiated by opening the valve to the mechanical vacuum pump and adjusting the syringe pumping rate so as to maintain the interface at a constant height. Under these conditions, the interface shape did not deviate from a spherical shape by more than 1% and the rate at which the liquid was pumped into the throat of the funnel was equal to the rate at which the liquid evaporated. The pumping rate could be set at a particular value with the pump controls and had a possible error of ±1% (manufacturer specification). The pumping rate was also checked by measuring the movement of the syringe plunger with a cathetometer. The measurements agreed closely with the set values.

The interface height was monitored with a cathetometer that had a resolution of ±10 μm. If the interface did not move a detectable amount during the course of an experiment, the evaporation was assumed to have been steady state. The pressure in the vapor phase was monitored at a position 20 cm above the mouth of the funnel with a Hg manometer that could be read with a cathetometer to an accuracy of ±0.1 mm or ±13.3 Pa. Once the conditions had been adjusted so D_2O was evaporating under steady-state conditions, two types of experiments were run. The conditions under which the first experimental series was performed are summarized in Table I and the second in Table II.

III. FIRST EXPERIMENTAL SERIES: MEASUREMENT OF THE SURFACE-THERMAL CAPACITY

In each experiment of the first series, the temperature field near the interface in both the liquid and vapor phases were measured with a U-shaped thermocouple (25.4-μm-diam wire, 46-μm-diam bead) that had been attached to a micropositioner enclosed in the chamber. The positioner could be moved in three dimensions from outside the chamber. The positioner was used to place the thermocouple bead on the center line in the vapor, and the thermocouple output recorded each second for 1 min (by a Labview program via a 34970A Aglient data acquisition/switch unit). The mean standard deviation (±SDV) temperature was recorded by comparing the thermocouple output with a previously recorded calibration curve. After a measurement, the positioner was used to lower the thermocouple toward the interface and the temperature recorded again. Near the interface, the distance between two measurements was 10 μm in the vapor phase. On the center line in the liquid phase, the thermocouple was first positioned immediately below the interface, the temperature recorded there, and then moved downward in 20-μm steps and the temperature recorded at each position. After the temperature had been measured on the center line, the thermocouple was moved in one horizontal direction successively to 0.7, 1.4, 2.1, 2.8, and 3.15 mm from the center line, and at each position, the temperature measured as a function of height following the same procedure as that used on the center line. When the measurements in one horizontal direction had been completed, without opening the apparatus, the thermocouple was brought back to the center line and the series of temperature measurements repeated, but with the thermocouple moved in a second horizontal direction separated from the first by 90°.

As may be seen in Fig. 1, the average, steady-state evaporation flux $\overline{j_{ev}}$ increased almost linearly as the (average) vapor-phase pressure was reduced in the different experiments. However, the extent to which the vapor-phase pressure could be reduced was limited. When attempts were made to reduce the vapor-phase pressure below 253.3±13.3 Pa (Table I, EVD11), the liquid spontaneously froze.

The Marangoni number was found to be the nondimensional parameter that characterized the interfacial flow in the case of H_2O [2]. If the liquid-vapor surface tension is denoted as γ^{LV}, the temperature of the water at the funnel throat by T_t^L, the thermal diffusivity of the liquid by α_L, the dynamic liquid viscosity by η_L, and the distance on the center

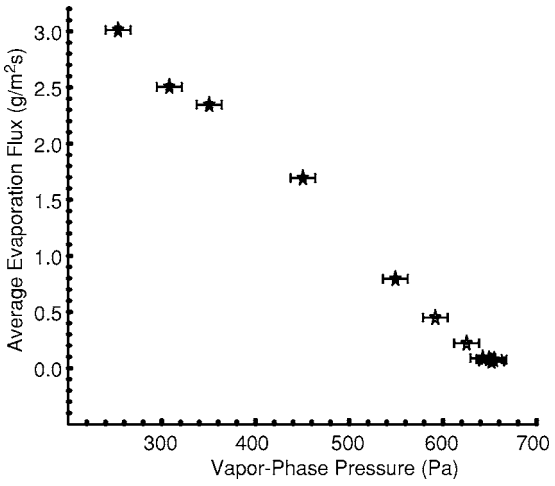

FIG. 1. Dependence of the average evaporation flux on the vapor-phase pressure for the experiments described in Table I.

TABLE I. Thermal conditions in liquid and vapor-phases measured during steady-state evaporation.

Experiment	EVD1	EVD2	EVD3	EVD4
Vap.-Ph. Press. (Pa)	651.9±13.3	654.6±13.3	649.3±13.3	642.6±13.3
Intf. Ht.[a] (mm)	1.00±0.01	0.98±0.01	0.98±0.01	0.98±0.01
Intf. Radius R_0 (mm)	6.63±0.09	6.74±1.00	6.74±1.00	6.74±1.00
Avg. Evap. Flux (g/m^2 s)	0.059±0.001	0.074±0.001	0.081±0.001	0.089±0.001
Throat temp. (°C)	3.60±0.02	3.66±0.03	3.59±0.02	3.58±0.02
T_I^V (°C)[a]	4.61±0.02	4.76±0.02	4.56±0.05	4.51±0.02
T_I^L (°C)[a]	3.61±0.02	3.65±0.02	3.58±0.03	3.44±0.02
Unif.-temp. layer[a] (mm)				
Ma	5.2	39.5	69.1	297.9
x_p/x_m	0.297	0.297	0.207	0.297
Tangential speed at x_p/x_m				

Experiment	EVD5	EVD6	EVD7	EVD8
Vap.-Ph. Press. (Pa)	625.3±13.3	591.9±13.3	549.3±13.3	450.6±13.3
Intf. Ht.[a] (mm)	1.00±0.01	1.00±0.01	1.00±0.01	1.00±0.01
Intf. Radius R_0 (mm)	6.63±0.09	6.63±0.09	6.63±0.09	6.63±0.09
Avg. Evap. Flux (g/m^2 s)	0.221±0.002	0.450±0.005	0.796±0.008	1.693±0.017
Throat temp. (°C)	3.61±0.02	3.57±0.03	3.63±0.02	3.69±0.04
T_I^V (°C)[a]	4.22±0.02	3.51±0.05	2.47±0.03	−1.46±0.03
T_I^L (°C)[a]	3.04±0.03	2.31±0.03	1.26±0.03	−0.15±0.03
Unif.-temp. layer[a] (mm)	0.41±0.01	0.23±0.02	0.12±0.01	0.09±0.02
Ma	1,267	2,649	4,869	9,244
x_p/x_m	0.297	0.297	0.300	0.306
Tangential speed at x_p/x_m	0.202	0.198	0.297	0.347

Experiment	EVD9	EVD10	EVD11
Vap.-Ph. Press. (Pa)	350.6±13.3	308.0±13.3	253.3±13.3
Intf. Ht.[a] (mm)	1.02±0.01	1.00±0.01	1.01±0.01
Intf. Radius R_0 (mm)	6.51±0.09	6.63±0.09	6.57±0.09
Avg. Evap. Flux (g/m^2 s)	2.346±0.023	2.506±0.022	3.012±0.030
Throat temp. (°C)	3.72±0.06	3.64±0.06	3.66±0.08
T_I^V (°C)[a]	−2.68±0.04	−4.45±0.07	−6.54±0.06
T_I^L (°C)[a]	−4.76±0.03	−6.69±0.03	−9.21±0.03
Unif.-temp. layer[a] (mm)	0.07±0.01	0.04±0.02	0.03±0.01
Ma	13,385	14,697	16,134
x_p/x_m	0.306	0.300	0.294
Tangential speed at x_p/x_m	0.354	0.372	0.303

[a]On the center line.

line from the throat thermocouple to the liquid-vapor interface by D, the Marangoni number may be expressed

$$\mathrm{Ma} = \frac{\left(\frac{d\gamma^{LV}}{dT^L}\right)_I (T_{0I}^L - T_I^L) D}{\alpha_L \eta_L}, \tag{1}$$

where the value of T_{0I}^L is calculated from the measured slope of the temperature in the liquid phase. In other words, it is the temperature that would exist at the interface if the measured, constant gradient in the temperature were stable [6]. (We note there are different definitions of the Marangoni number used in the literature. For example, the definition used in [24] is different from that in [6]. We adopt the one introduced by Pearson [6]. In which case, the critical Marangoni number indicates the maximum linear temperature gradient that can be sustained in a horizontal liquid layer heated from below without the onset of thermocapillary convection. Pearson found the critical Marangoni number to be ~80.)

For the set of experiments described in Table I, Ma is shown in Fig. 2, and for comparison, the results reported for H_2O [2] are also shown. The temperature field near the in-

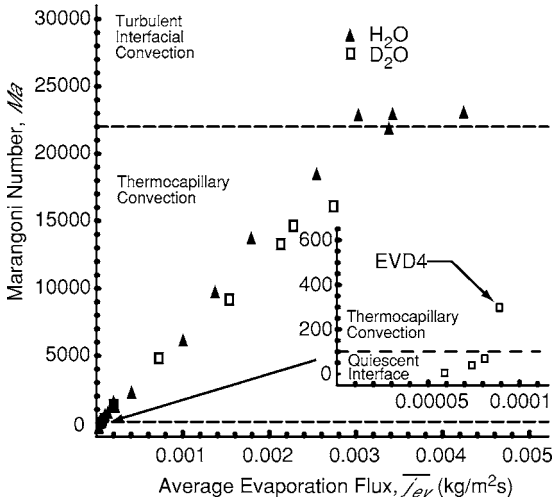

FIG. 2. Marangoni number for the experiments with different evaporation fluxes. The results obtained with D_2O (Table I) and for H_2O that were previously reported [2].

terface depended strongly on the evaporation flux or value of Ma. For the experiments EVD1–EVD3 (Table I) for which Ma was less than 100, the type of results obtained is illustrated in Fig. 3. Note that the temperature in the liquid phase was uniform, but there was an interfacial temperature discontinuity in which the interfacial vapor temperature was greater than that of the liquid phase. The liquid was evaporating as a result of the heating through the vapor phase by the room-temperature surroundings.

The Marangoni number for experiments EVD4–EVD11 was in the range $100 < \mathrm{Ma} < 17{,}000$. A temperature field measured in these experiments is shown in Fig. 4. Note that along the interface, there was an interfacial temperature discontinuity, the temperature in the liquid immediately below the interface was uniform with depth, and below the uniform-temperature layer the temperature gradient with depth was constant.

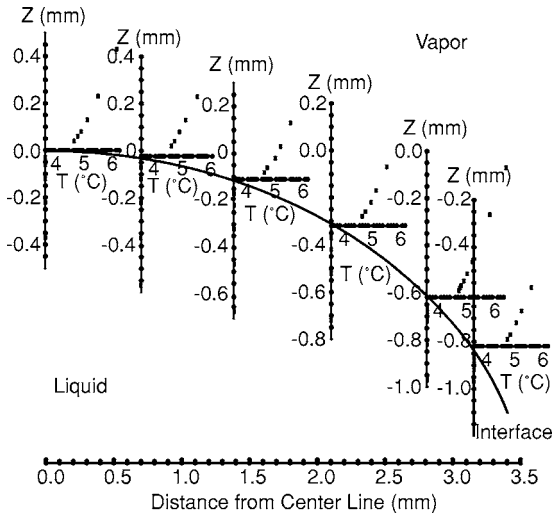

FIG. 3. Measured temperatures in one horizontal direction in both the liquid and vapor phases during the steady-state evaporation of D_2O (EVD1, Table I).

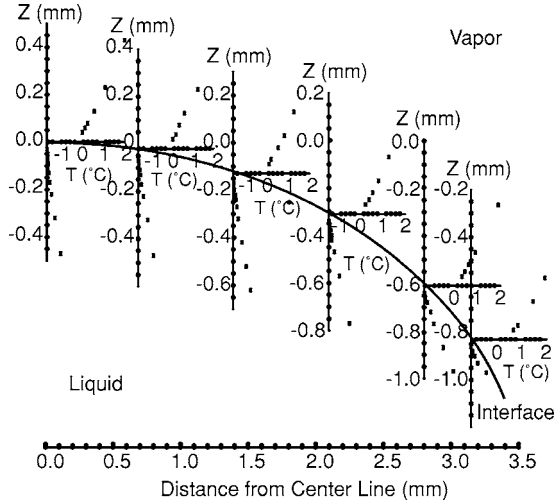

FIG. 4. Measured temperatures in one horizontal direction in both the liquid and vapor phases during the steady-state evaporation of D_2O (EVD8, Table I).

These features of the temperature field for experiment EVD8 are shown in Fig. 5. Note that the interfacial liquid temperature indicates that the temperature field was axisymmetric and suggests that thermocapillary-induced flow from the periphery toward the center line would be present. The uniform-temperature layer is seen to have its maximum depth at the center line and minimum at the periphery.

The temperature field will be described in spherical coordinates $(r, \theta, \phi$ where ϕ is the azimuthal angle measured about the axis with polar angle θ equal to 0°). It was found

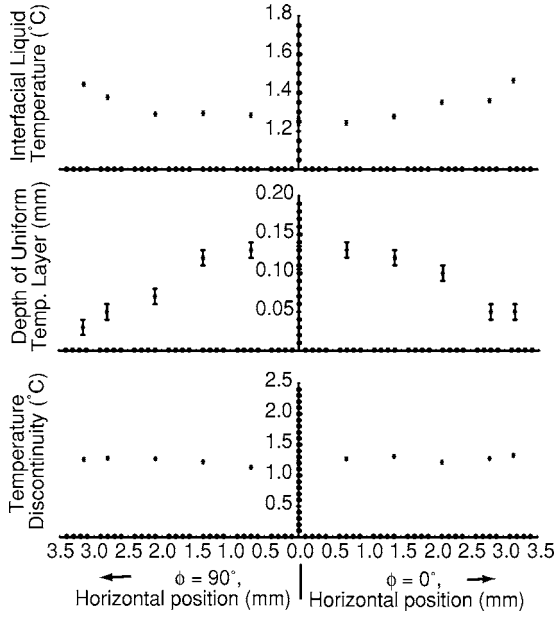

FIG. 5. The measured interfacial liquid temperature during EVD8 (Table I) is shown in the upper graph. The depth of the uniform-temperature layer during this experiment is shown in the middle graph, and the measured interfacial temperature discontinuity in which the interfacial vapor temperature was greater than that in the liquid phase is shown in the lower graph.

that the interfacial liquid temperature T_I^L in all the experiments could be represented by

$$T_I^L = a_0 + a_1 \sin^2 \theta, \tag{2}$$

where the values of the coefficients a_0 and a_1 were determined from the measured interfacial temperature profile in each experiment. We note the same type of empirical relation was used to describe the interfacial temperature profile during water evaporation [1]. If the thermal conductivity of phase j is denoted κ^j, the net thermal energy flux to the interface is given by

$$q_N = \kappa^V \left(\frac{\partial T^V}{\partial r} \right)_I - \kappa^L \left(\frac{\partial T^L}{\partial r} \right)_\delta, \tag{3}$$

where a subscript I indicates the quantity is to be evaluated at the interface and a subscript δ indicates the quantity is to be evaluated at the bottom of the uniform temperature layer. By evaluating the partial derivative at the latter position, it is being assumed that since the system is operating in steady state, the energy thermally conducted to the bottom of the uniform temperature layer is transported by fluid mixing in the uniform temperature layer (see below) to the interface where the phase change takes place. Since the temperature was measured in the vertical direction, q_N is evaluated from

$$q_N = \frac{\kappa^V}{\cos \theta} \left(\frac{\partial T^V}{\partial z} \right)_I - \frac{\kappa^L}{\cos \theta} \left(\frac{\partial T^L}{\partial z} \right)_\delta. \tag{4}$$

It was found that for each experiment that the experimental values of q_N could be expressed as

$$q_N = c_0 + c_1 \cos \theta + c_2 \cos^2 \theta + c_3 \cos^3 \theta, \tag{5}$$

where the values of $c_j (0 \leqslant j \leqslant 3)$ for each experiment were determined from the measured slopes on the center line and at ten additional positions along the interface (see Fig. 5). The same type of empirical relation was used to calculate the thermal flux to the interface in the case of water [2].

The total thermal energy transport to the interface from the axisymmetric temperature field, $\dot{Q}_N$, is given by

$$\dot{Q}_N = 2\pi \int_0^{\theta_m} q_N R_0^2 \sin \theta \, d\theta, \tag{6}$$

where R_0 is the radius of the interface and θ_m is the maximum polar angle of the interface. If the radius of the funnel mouth is denoted as x_m, this angle may be determined from

$$\theta_m = \sin^{-1} \left(\frac{x_m}{R_0} \right). \tag{7}$$

Since the rate of evaporation, J_{ev}, could be directly measured by measuring the pumping rate, the rate of energy transport to the interface required to evaporate the liquid at the measured rate $\dot{E}_{ev}$ may be expressed in terms of enthalpies of the liquid and vapor phases—h^L and h^V, respectively—evaluated at the interfacial conditions in the respective phases:

$$\dot{E}_{ev} = J_{ev} (h^V - h^L)_I. \tag{8}$$

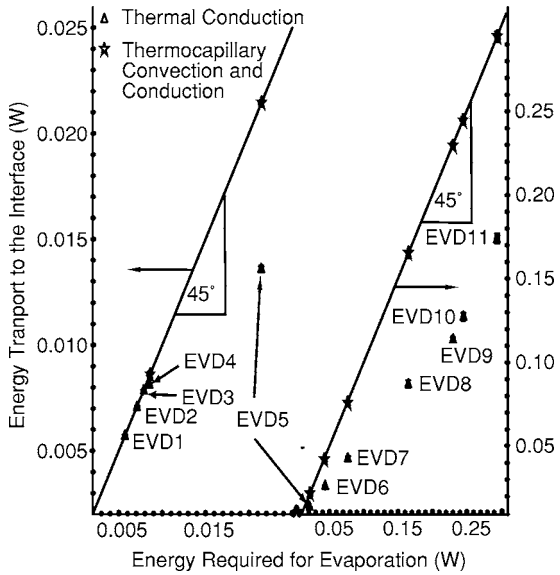

FIG. 6. Calculated energy transport to the interface by thermal conduction and by the thermocapillary convection and thermal conduction compared with the energy transport rate required to evaporate the liquid at the measured rate.

If the energy transport to the interface is by thermal conduction alone, then $\dot{Q}_N$ and $\dot{E}_{ev}$ must be equal. In Fig. 6, $\dot{Q}_N$ and $\dot{E}_{ev}$ are compared for each of the experiments described in Table I. As may be seen there, at the lowest evaporation rates EVD1–EVD3 ($0.006 \text{ W} \leqslant \dot{E}_{ev} \leqslant 0.007 \text{ W}$), $\dot{Q}_N$ and $\dot{E}_{ev}$ are equal. Thus, for experiments with mean evaporation fluxes in the range $0.059 \leqslant \overline{j_{ev}} \leqslant 0.081 \text{ g/(m}^2 \text{ s)}$, thermal conduction provides the energy required to evaporate the liquid at the observed rate. The Marangoni number for these experiments was in the range $5 < \text{Ma} < 70$; however, when the evaporation rate was increased so that Ma reached 298, the energy transported to the interface by thermal conduction was less than that required to evaporate the liquid at the measured rate. And as the evaporation rate was progressively increased further, as seen in Fig. 6, the energy transport by thermal conduction provided a progressively smaller portion of energy required to evaporate the liquid. At the highest evaporation rate, thermal conduction provided less than 60% of the required energy transport.

A. Thermocapillary energy transport during D_2O evaporation

The results shown in Fig. 6 suggest that there is an active energy transport mechanism besides thermal conduction, and the results in Fig. 5 indicate that thermocapillary convection would be present. We follow the procedure outlined in [2] to determine the value of the surface-thermal capacity c_σ for D_2O using measurements reported in Table I. If the Gibbs [7] excess model of the interface is used to define the excess number of moles and the excess internal energy, the conservation principles may be applied to develop an analytical expression for the surface-thermal capacity.

If the density and velocity in the bulk phases, evaluated at the interface, are denoted n_I^L, $\boldsymbol{\nu}_I^L$, n_I^V, and $\boldsymbol{\nu}_I^V$, respectively, and the evaporation flux j_{ev} is defined by

$$j_{ev} = n^L \boldsymbol{\nu}_I^L \cdot \boldsymbol{i}_r = n^V \boldsymbol{\nu}_I^V \cdot \boldsymbol{i}_r, \tag{9}$$

then, if the thermocapillary speeds are denoted ν_θ^{LV} and ν_ϕ^{LV}, molecular conservation in the interface phase maintained at steady state gives

$$\boldsymbol{\nabla}(n^{LV}\nu_\theta^{LV}) \cdot \boldsymbol{i}_\theta + \boldsymbol{\nabla}(n^{LV}\nu_\phi^{LV}) \cdot \boldsymbol{i}_\phi = 0. \tag{10}$$

If the temperature of the surface phase is denoted as T^{LV} and the interface radius as R_0, when conservation of energy is imposed at the interface, one finds

$$j_{ev}(h^V - h^L)_I = (\kappa^V \boldsymbol{\nabla} T^V - \kappa^L \boldsymbol{\nabla} T^L)_I \cdot \boldsymbol{i}_r - \frac{c_\sigma \nu_\theta^{LV}}{R_0}\left(\frac{\partial T^{LV}}{\partial \theta}\right) - \frac{c_\sigma \nu_\phi^{LV}}{R_0}\left(\frac{\partial T^{LV}}{\partial \phi}\right) - \Phi_I. \tag{11}$$

We neglect any difference between T_I^L and T^{LV}, assume the liquid phase temperature field is axisymmetric, and neglect the viscous dissipation; then, Eq. (11) simplifies to

$$j_{ev}(h^V - h^L) = (\kappa^V \boldsymbol{\nabla} T^V - \kappa^L \boldsymbol{\nabla} T^L)_I \cdot \boldsymbol{i}_r - \frac{c_\sigma \nu_\theta^{LV}}{R_0}\left(\frac{\partial T^{LV}}{\partial \theta}\right). \tag{12}$$

For an interfacial element maintained at steady-state, Eq. (12) may be understood physically: the first term on the left is the energy flux required to evaporate liquid at the flux rate of j_{ev}, the second term is the thermal-conduction flux to the surface element, and the third is the thermal energy transport by thermocapillary convection. To apply the third term, the value of the thermocapillary speed, ν_θ^{LV}, must be evaluated. An expression for this quantity has been previously developed [1]:

$$\nu_\theta^{LV} = -\frac{1}{\eta_L}\left(\frac{d\gamma^{LV}}{dT_I^L}\right)\left(\frac{dT_I^L}{d\theta}\right)\ln\left(1 - \frac{\delta_u}{R_0}\right), \tag{13}$$

where δ_u is the depth of the uniform-temperature layer. When the liquid was evaporating at a steady rate, the depth of the uniform-temperature layer depended on position. (For example, see Fig. 5.) It has been found that the depth of this layer during water evaporation can be represented by [1]

$$\delta_u = b_0 + b_1 \sin^2\theta + b_2 \sin^4\theta. \tag{14}$$

We shall assume the same relation is valid for $D_2O(l)$ evaporation. This assumption is examined in a subsequent section. The values of $b_j (0 \leqslant j \leqslant 2)$ are determined from the measured temperature profiles of each experiment. The values of the thermocapillary speeds calculated at approximately the same horizontal distance from the center line for each experiment are listed in Table I.

In the experiments described in Table I, the temperature along the interface varied by a fraction of a degree–C; thus, we shall assume that in any one experiment, the surface-thermal capacity is constant. With this assumption Eq. (12) may be integrated over the interface and solved for the surface-thermal capacity to obtain

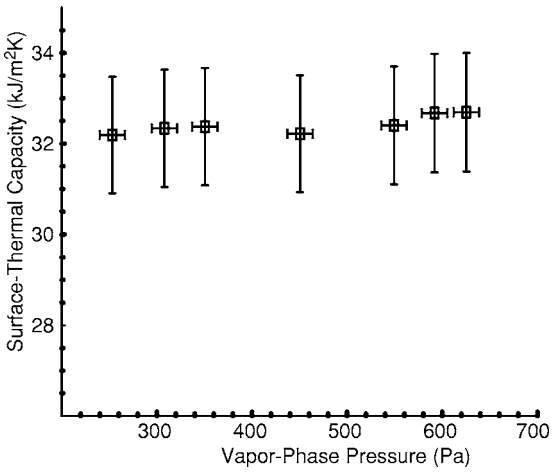

FIG. 7. Comparison of the values of the surface-thermal capacity determined for the experiments defined in Table I.

$$c_\sigma = \frac{(\dot{Q}_N - \dot{E}_{ev})}{2\pi R_0 \int_0^{\theta_m} \nu_\theta^{LV}\left(\frac{\partial T^{LV}}{\partial \theta}\right)\sin\theta\, d\theta}. \tag{15}$$

After making use of Eqs. (2), (6), (8), and (13) and the results in Table I, one finds the values of the surface-thermal capacity shown in Fig. 7. Although Ma changed by an order of magnitude and the evaporation rate by a factor of 3 in these experiments (Table I), as seen in Fig. 7, the value of the surface-thermal capacity did not change measurably from the mean of 32.5 kJ/(m^2 K). The error in the measured value of c_σ has been estimated, following the procedure outlined in [2,3]. A value of ±2.5% is found. Thus we take the value of c_σ to be 32.5±0.8 kJ/(m^2 K) for D_2O when the temperature is in the range $-10 \leqslant T^{LV} \leqslant 3.7$ °C.

Once the value of c_σ is known, the value of the total energy transport rate to the surface by thermal conduction and by thermocapillary convection can be directly calculated,

$$\dot{Q}_N - 2\pi R_0 \int_0^{\theta_m} c_\sigma \nu_\theta^{LV}\left(\frac{\partial T^{LV}}{\partial \theta}\right)\sin\theta\, d\theta,$$

and compared with that required to evaporate the liquid at the measured rate $\dot{E}_{ev}$, Eq. (8). As seen in Fig. 5, for the inferred value of c_σ, the energy conservation principle is completely satisfied when both thermocapillary convection and thermal convection are considered as the modes of energy transport.

B. Local evaporation flux

Once the value of c_σ is known, Eq. (12) may be combined with Eqs. (2), (5), (13), and (14) and the local evaporation flux calculated. One finds the results shown in Fig. 8. Note that for experiments EVD1–EVD3, the calculated evaporation flux was uniform. For these three experiments, Ma < 70 and the energy analysis indicated that the thermal conduction to the interface provided the energy required to

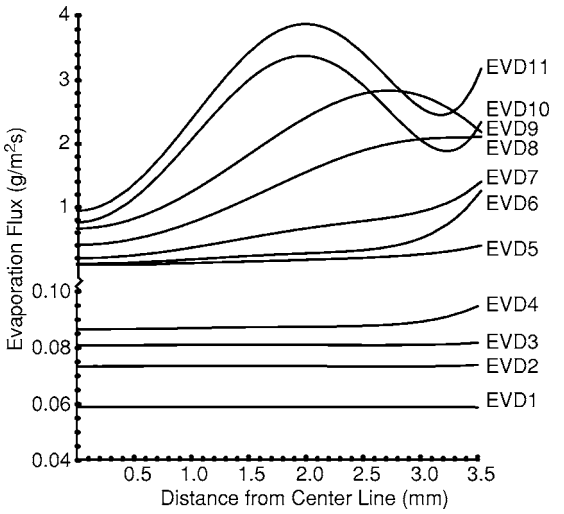

FIG. 8. Calculated evaporation flux as a function of the distance from the center line for the experiments defined in Table I.

evaporate the liquid at the observed rate (see Fig. 6). As the evaporation rate was increased (EVD4–EVD11), the calculated evaporation flux became progressively more nonuniform, and in these experiments, the energy analysis indicated that thermocapillary convection played a progressively more important role in the energy transport. In experiments EVD4–EVD8, the maximum evaporation flux was at the periphery of the circular cone. However, in experiments EVD9, EVD10, and EVD11, the maximum evaporation flux moved toward the center line of the funnel.

C. Interaction of the thermal, flow, and pressure fields

The evaporation flux is a reflection of the energy transport to the interface and the pressure in the vapor phase; thus, to understand why the maximum evaporation flux moves toward the center line as the evaporation rate is increased, the temperature, flow, and pressure fields must be considered. The net thermal conductive flux calculated from Eq. (5) is shown in Fig. 9. As seen there, for those experiments in which the interface was quiescent (Ma$<$100) the thermal conduction to the interface was uniform, but as the evaporation rate was increased, the thermal conduction to the interface became nonuniform with its maximum at the periphery of the stainless-steel funnel. This is the expected result, since the thermal conductivity of the stainless steel is $\sim$27 times higher than that of D_2O at 0 °C and the temperature at the funnel throat was maintained $\sim$3.65 °C in each experiment.

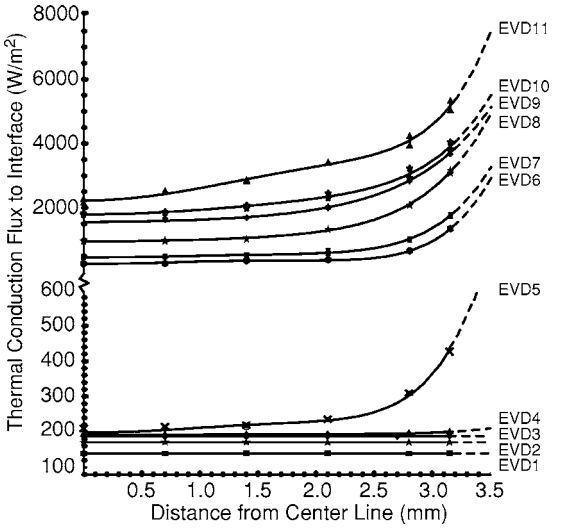

FIG. 9. Calculated net thermal conductive flux to the interface as a function of distance from the center line is shown. The data points indicate the measured values used to determine the empirical constants in Eq. (5). The funnel mouth was 3.5 mm in diameter. The thermocouple could not be placed more than 3.15 mm from the center line. The dashed lines indicated the extrapolated portions of the calculations.

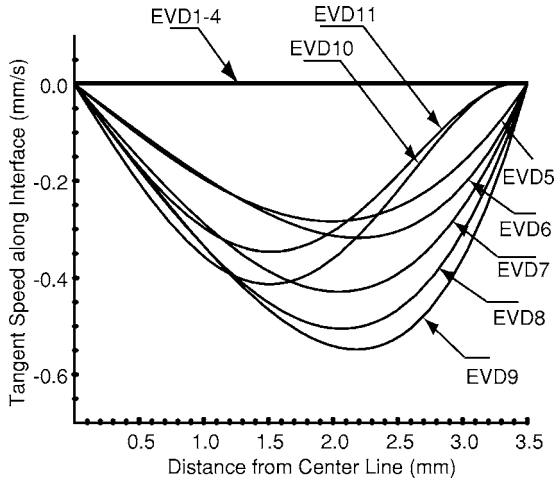

FIG. 10. The thermocapillary-generated fluid speed ν_θ^{LV} is shown for the experiments described in Table I.

For the experiments described in Table I, the fluid speed ν_θ^{LV} calculated from Eq. (13) is shown in Fig. 10. Note that ν_θ^{LV} goes to zero at the solid funnel wall because the uniform-temperature layer thickness goes to zero there [see Eq. (13)] and ν_θ^{LV} also goes to zero on the funnel center line, since the temperature gradient goes to zero there. Provided that Ma for an experiment was greater than 100, ν_θ^{LV} reaches a maximum between the center line and the funnel periphery. Since energy transport by thermocapillary convection is so important at the higher evaporation rates, the results in Fig. 10 suggest that the reason the evaporation flux has a maximum between the center line and the periphery in experiments EVD9, EVD10, and EVD11 is because the thermocapillary speed is a maximum in the same region for these experiments.

As seen in Fig. 1, lowering the (average) vapor-phase pressure had the effect of increasing the average evaporation flux. Since the evaporation flux was higher at the periphery than on the center line, this might be expected to mean that the pressure would be "lower" at the periphery. This could be viewed as paradoxical: since, as indicated in Fig. 10, the thermocapillary speed was from the periphery to the center line; hence, the no-slip boundary condition would suggest that the interfacial vapor flow should also be from the peririphery to the center line. But if the pressure is *lower* at the periphery than at the center line, why would the flow be *from* the periphery toward the center line?

To examine this apparent paradox, we use statistical rate theory [8–20] to predict the vapor-phase pressure along the interface. From this theoretical approach one finds that the local vapor-phase pressure on the interface can be expressed in terms of measurable parameters j_{ev}, T_I^L, T_I^V, and R_0:

$$P_I^V = P_s(T_I^L) - \frac{2\gamma^{LV}}{R_0} + \left(\frac{k_B T_I^L}{v_s^L(T_I^L)}\right)\left\{\sinh^{-1}\left(\frac{j_{ev}}{2K_e}\right) - 4\left(1 - \frac{T_I^V}{T_I^L}\right)\right.$$

$$- \left(\frac{1}{T_I^V} - \frac{1}{T_I^L}\right)\sum_{l=1}^{3}\left(\frac{\hbar\omega_l}{2k_B} + \frac{\hbar\omega_l/k_B}{\exp\left(\frac{\hbar\omega_l}{k_B T_I^L}\right) - 1}\right)$$

$$\left. - \ln\left[\left(\frac{T_I^V}{T_I^L}\right)^4\left(\frac{P_s(T_I^L)}{P_I^V}\right)\left(\frac{q_{\text{vib}}(T_I^V)}{q_{\text{vib}}(T_I^L)}\right)\right]\right\}, \tag{16}$$

where (1) the subscript s on a property indicates the property is to be evaluated at the saturation condition of the liquid and vapor phases across a flat surface when they are at the indicated temperature and (2) the vibrational partition function $q_{\text{vib}}(T_I^V)$ may be expressed in terms of the measured values of the fundamental vibration frequencies ω_l of the D_2O molecule: 1,178.38, 2,669.4, and 2,787.92 cm^{-1} [25]:

$$q_{\text{vib}}(T_I^V) = \prod_{l=3}^{3}\frac{\exp(-\hbar\omega_l/2k_B T_I^V)}{1 - \exp(-\hbar\omega_l/k_B T_I^V)}; \tag{17}$$

K_e is given by

$$K_e = \frac{P_s(T_I^L)\exp\left[\frac{v_s^L(T_I^L)}{k_B T_I^L}[P_{0e}^L - P_s(T_I^L)]\right]}{\sqrt{2\pi m_{D_2O} k_B T_I^L}}, \tag{18}$$

where P_{0e}^L is determined iteratively from

$$P_{0e}^L = P_s(T_I^L)\exp\left[\frac{v_s^L(T_I^L)}{k_B T_I^L}[P_{0e}^L - P_s(T_I^L)]\right] + \frac{2\gamma^{LV}(T_I^L)}{R_0}. \tag{19}$$

We emphasize that there are no unspecified parameters in the coupled system of equations (16)–(19). All of the parameters have been previously and independently measured.

Since the values of T_I^L, T_I^V, and R_0 have been directly measured and the local values of j_{ev} have been calculated, as indicated in Fig. 8, the vapor-phase pressure on the interface may be calculated from Eqs. (16)–(19) and the properties of D_2O listed in the Appendix. For the 11 experiments described in Table I, one finds the results shown in Fig. 11. Note that in experiments EVD1–EVD8, there was no significant pressure gradient, but in each of the other experiments, the gradient in pressure is in the same direction as the thermocapillary flow; thus, there is no paradox.

In Fig. 12, the average vapor-phase pressure on the interface calculated from Eqs. (16)–(19) is compared with the pressure measured in the vapor phase. The vertical error bars are the possible measurement error in the manometer reading, 13.3 Pa, and the horizontal error bars are the standard deviation in the vapor-phase pressure calculated along the interface (see Fig. 11). The increase in these error bars with a decrease in the vapor-phase pressure is a reflection of the gradient in the vapor-phase pressure along the interface that develops with the increase in the thermocapillary speed.

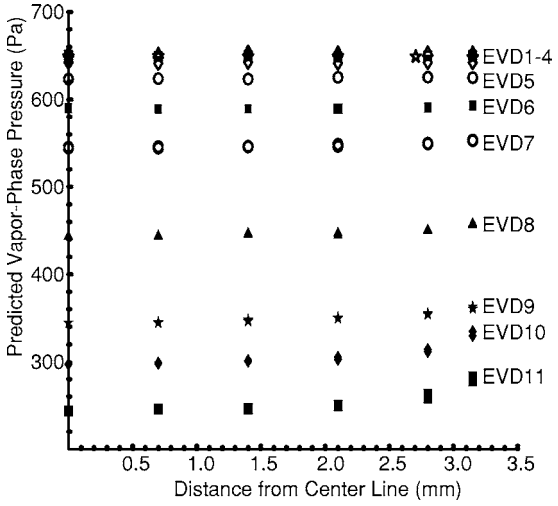

FIG. 11. The vapor-phase pressure on the interface predicted from statistical rate theory at each point on the interface where the interfacial temperatures T_I^L and T_I^V were measured. The values of R_0 and j_{ev} were also used in the calculations.

IV. SECOND EXPERIMENTAL SERIES: MEASUREMENT OF THERMOCAPILLARY FLOW SPEED AND CHARACTERICS

In the analysis outlined in the previous sections, the value inferred for c_σ depended inversely on the thermocapillary speed v_θ^{LV} [see Eq. (15)], but the value of v_θ^{LV} could not be measured directly; nor could the nature of the interfacial flow

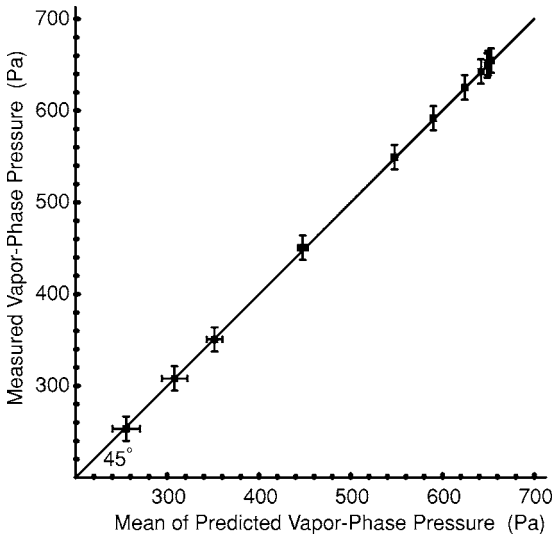

FIG. 12. The measured vapor-phase pressure is compared with the average of the vapor-phase pressure along the interface calculated with statistical rate theory.

TABLE II. Thermal conditions existing in probe deflection experiments. (Probe modulus of elasticity E: 141.13±0.79 GN/m^2. Probe density: 8.73×10^3 kg/m^3. Probe length L: 42 mm. Probe diameter D_p: 12.7 μm. Probe immersion depth: 40 μm.)

Experiment	EVD12	EVD13	EVD14	EVD15
Vapor-phase pressure (Pa)	651.9±13.3	590.6±13.3	549.3±13.3	452.0±13.3
Max. interface height (mm)	1.00±0.01	1.00±0.01	1.00±0.01	1.00±0.01
Intf. radius R_0 (mm)	6.63±0.09	6.63±0.09	6.63±0.09	6.63±0.09
Evaporation flux (g/m^2 s)	0.059±0.001	0.450±0.005	0.796±0.008	1.693±0.017
Throat temperature TC3 (°C)	3.60±0.02	3.57±0.02	3.63±0.02	3.69±0.03
Probe position (x_p/x_m)	0.297	0.297	0.300	0.306
Mean probe deflection y_p (pixels)	0	0.533±0.503	0.717±0.667	1.017±0.792
Max. probe amplitude (pixels)	0	1±1	2±1	3±1
Tangential speed from mean probe deflection (mm/s)	0	0.169±0.158	0.226±0.207	0.287±0.217
Tangential speed from surface tension (mm/s)	0	0.198	0.297	0.347

Experiment	EVD16	EVD17	EVD18
Vapor-phase pressure (Pa)	350.6±13.3	308.0±13.3	254.6±13.3
Max. interface height (mm)	1.02±0.01	1.00±0.01	1.01±0.01
Intf. radius R_0 (mm)	6.51±0.09	6.63±0.09	6.57±0.09
Evaporation flux (g/m^2 s)	2.346±0.023	2.506±0.022	3.012±0.030
Throat temperature TC3 (°C)	3.72±0.03	3.64±0.03	3.66±0.03
Probe position (x_p/x_m)	0.306	0.300	0.294
Mean probe deflection y_p (pixels)	1.350±0.820	1.833±0.942	1.817±1.255
Max. probe amplitude (pixels)	3±1	4±1	5±1
Tangential speed from mean probe deflection (mm/s)	0.329±0.193	0.407±0.200	0.362±0.242
Tangential speed from surface tension (mm/s)	0.354	0.372	0.303

could be assessed in the first series of experiments. To compare the calculated value of ν_θ^{LV} with measurements, a second set of experiments, described in Table II, was conducted. The same experimental protocol was used as in the first set: the temperature at the funnel throat and the vapor phase pressures were set at approximately the same values as in the first set.

To measure the thermocapillary speed, the thermocouple that had been mounted on the micropositioner was replaced with a vertically oriented, cantilevered probe. The probe tip was immersed 40 μm, I_d into the evaporating liquid, and the deflection of the tip, y_p, measured as a function of time. To determine the probe deflection, its image was recorded just before the tip was immersed. Afterwards, the position of the probe tip was recorded every 0.5 s for a period of 30 s using a video camera mounted on a telescope, and the images were analyzed by NIH Image 1.61/68 K. From each image, the position of the probe tip was determined relative to the position 40 pixels above the tip and taken to be the value of the tip deflection at each of the these 60 times. The mean (±SDV) of the probe deflection for each experiment of the second set is listed in Table II, and in Fig. 13, the probe deflection as a function of time for three experiments is shown.

For low Reynolds number flow of an incompressible liquid, having a density n^L and a dynamic viscosity of η_L flowing perpendicular to the axis of a cylinder of infinite length and diameter D_p, the drag per unit length, F_d, in the Oseen approximation is given by [26]

$$F_d = \frac{4\pi\eta_L\nu_\theta^{LV}}{0.077 + \ln\left(\frac{n^L\nu_\theta^{LV}D_p}{8\eta_L}\right)}. \tag{20}$$

The force F_c required to deflect the tip of a cantilevered beam that has an elastic modulus of E, a diameter D_p, and a length L a distance y_p is given by

$$F_c = \frac{3\pi E D_p^4 y_p}{64L^3}. \tag{21}$$

After multiplying F_d by the immersion depth of the probe, I_d, and equating the result to the force required to deflect the tip a distance y_p, one finds [1]

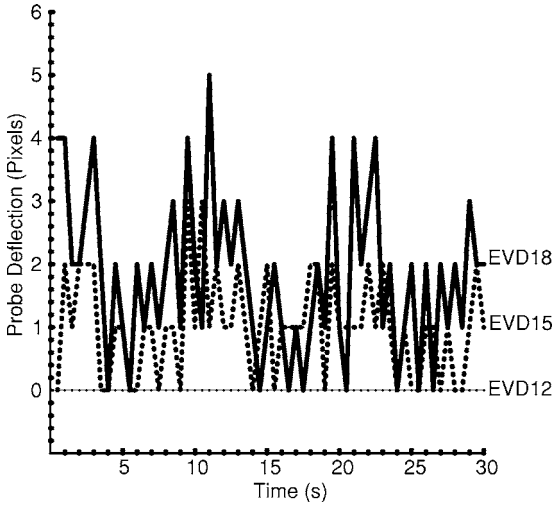

FIG. 13. The deflection of the tip of a small probe immersed into the liquid as it evaporated under steady-state conditions during three different experiments (see Table II).

$$\nu_\theta^{LV} - \left(\frac{3EI_d y_d}{4\pi\eta_L I_d L^3}\right)\ln\left(\frac{n^L D_p \nu_\theta^{LV}}{8\eta_L}\right) = \frac{0.231 E D_p^4 y_p}{256\eta_L I_d L^3}. \quad (22)$$

From the measured, mean probe deflections listed in Table II, the value of ν_θ^{LV} may be calculated iteratively from Eq. (22) for each experiment. Also listed there is the value of ν_θ^{LV} calculated from the surface tension gradient of the corresponding experiment in the first set of experiments, Table I. Note that the two values calculated for ν_θ^{LV} agree well. This agreement indicates that it was temperature (or surface-tension) gradient that gave rise to the flow measured by the probe. However, there were large fluctuations in the probe deflection about its mean displacement, as indicated in Fig. 13.

Experiment EVD12 (Table II) had a mean evaporation flux of 0.059 $g/(m^2\,s)$, the lowest of the second experimental series. As seen in Fig. 13, there were no measurable fluctuations of the probe, in this case. The conditions of this experiment corresponded with those of EVD1 (Table I), and in the latter experiment, the temperature in the liquid phase was found to be uniform both with depth and along the interface. Thus there would have been no thermocapillary convection. The thermal conduction through the vapor phase provided the energy required to evaporate the liquid at the measured rate (Fig. 6).

Compared with EVD12, the mean evaporation rate of EVD15 was ~29 times larger. The probe deflections and fluctuations were then clearly measurable, and when the evaporation flux was increased again in EVD18, so did the mean probe deflection and the fluctuation magnitude (Fig. 13). The power spectrum for experiments EVD12, EVD15, and EVD18 are shown in Fig. 14. Note that both spectra had peaks at the same frequencies. The dominate frequency in experiment EVD18 was at 0.133 Hz. There were peaks in the power spectra of the other experiments, either at this frequency or at one of its harmonics.

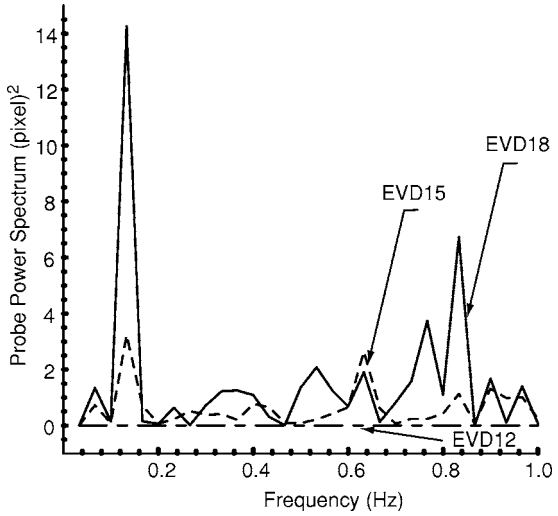

FIG. 14. Power spectrum of the probe deflection during experiments EVD12, EVD15, and EV18.

The natural frequency of the probe, ω_N, can be estimated from the relation [1]

$$\omega_N = \frac{1}{2\pi}\left(\frac{3D_p^2 E}{16L^4\rho_p}\right)^{1/2}. \quad (23)$$

After making use of the parameter values listed in Table II, one finds that the natural frequency of the probe is ~2 Hz or approximately 15 times the dominate frequency of EVD18. This suggests that the flow was oscillatory and that the frequency of the flow oscillations were repeating. However, we note that unlike the case with H_2O evaporation at larger rates, the power spectrum does not indicate an oscillation continuum; nor was there a bifurcation in the relation between the vapor-phase pressure and the mean evaporation flux. The absence of these characteristics seems consistent with the suggestion that there is no transition to a turbulent interfacial flow unless Ma exceeds 22,000 [1], and for the D_2O experiments the maximum value of Ma was ~16,000 (Table I).

V. DISCUSSION AND CONCLUSION

Qualitatively, the results are remarkably similar to those obtained for H_2O [1,2]: (1) When D_2O evaporated under conditions where Ma was less than ~100 (EVD1–EVD3, Table I), the temperature and evaporation flux were uniform along the interface (see Figs. 3 and 8), the interface was quiescent, and thermal conduction supplied the energy required to evaporate the liquid at the measured rate (see Fig. 6). (2) When the vapor-phase pressure was reduced while maintaining the temperature at the funnel throat at ~3.65 °C, Ma became greater than ~100 and a transition occurred at the interface. The interfacial liquid temperature became parabolic with its minimum on the center line of the spherical interface and its maximum at the funnel periphery (see Fig. 5). This steady-state temperature field gave rise to thermocapillary convection and a uniform-temperature layer

immediately below the interface (see Fig. 5). Below this layer, the temperature gradient was uniform. Thermal conduction to the interface through the liquid and vapor phase only accounted for a fraction of the energy required to evaporate the liquid at the measured rate. To calculate the energy transported to the interface through the liquid phase, it was assumed that the energy transported to the bottom of the uniform-temperature layer was transported across this layer by mixing. In other words, for the steady-state circumstance we consider, we suppose that there was no storage of energy in the uniform temperature layer. We emphasize that controlling the throat temperature at $\sim 3.65\ ^{\circ}\mathrm{C}$ eliminated any Marangoni-Bénard or roll-type convection [5].

As indicated by Eq. (13), the depth of the uniform temperature layer is related to the *mean* thermocapillary speed. The second series of experiments, conducted with the flow probe, was performed to examine this relation (see Table II). The value of the mean thermocapillary speed was calculated in two ways: one was to use the measured steady-state temperature gradient and the measured thickness of the uniform temperature layer in Eq. (13) (see Table I). The other was to assume that the probe deflection resulted from the drag force produced by the flow around the cylindrical probe and to equate this force to the elastic force required to deflect a cantilevered "beam." The root mean square of the difference in the mean value of ν_θ^{LV} determined by the two methods is 1.5%. This suggests that Eq. (13) gives a method by which reasonably accurate values of the mean value of ν_θ^{LV} may be determined. The fluctuation in the probe deflection indicates an oscillation in the flow speed of the same magnitude as the mean flow (Table II). However, the probe deflection never became negative, indicating that the flow was always in the same direction, but fluctuating in magnitude. Note that if ν_θ^{LV} is determined from Eq. (13), only the material properties of D_2O (see the Appendix) and the measured temperature profiles are required to calculate its value.

Once a method for determining the mean value of ν_θ^{LV} was available, the mechanisms by which energy is transported to the interface to evaporate the liquid can be investigated. As may be seen from Table I and Fig. 6, for the series of experiments with $298 \leqslant \mathrm{Ma} \leqslant 16{,}134$, as the evaporation rate was increased, thermal conduction provided a progressively *smaller* portion of the energy required to evaporate the liquid at the measured rate. At the highest evaporation rate, thermal conduction through the liquid and vapor phases provided less than 60% of the requite energy.

If the energy transport by thermocapillary convection is taken into account and c_σ is assigned a value of $32.5 \pm 0.8\ \mathrm{kJ/(m^2\,K)}$ (see Fig. 7), then as indicated in the series of seven experiments shown in Fig. 6, energy conservation is fully satisfied for each experiment. It appears energy is conducted from the throat of the stainless-steel funnel to its rim where the liquid-vapor interface is heated to give temperature profiles, such as that indicated in Fig. 5, and then the thermocapillary convection transports the energy along the interface.

Once the value of c_σ is known, the value of the local equilibrium flux j_{ev} can be calculated from the conservation equations. The values obtained from Eq. (12) are shown in Fig. 8, and once the value of j_{ev} is known, statistical rate theory may be used to calculate the vapor-phase pressure on the interface. Since statistical rate theory does not introduce any adjustable parameters, the predicted pressure may be directly compared with that measured. The mean value of the pressure on the interface agrees well with that measured 20 cm above the mouth of the conical funnel, as may be seen in Fig. 12. Further, the calculated pressure gradient in the vapor phase along the interface is consistent with a thermocapillary flow from the periphery toward the center line of the spherical interface (see Fig. 11).

One value of c_σ leads to conservation of energy being satisfied in each of seven experiments (see Fig. 6). When this value of c_σ is used with the conservation equations and statistical rate theory, that value of c_σ leads to the prediction of vapor-phase pressure values that, in each of the seven experiments, are consistent with the measured values, without the introduction of adjustable parameters. Thus the inferred value of c_σ has significant experimental support. Nonetheless, its inferred value is larger than would be expected for an equilibrium interface. The value of c_σ for H_2O was also larger than expected [2]. However, since the Gibbs model of the interface has been used to describe the surface phase, that is the expected result.

One of the physical characteristics that these two liquids have in common is their hydrogen bonding. Thus one could reasonably expect them to be approximately described by the "random network model" [21–23]. In this model, water is viewed as a hydrogen-bonded network with the molecules vibrating about their quasiequilibrium positions. The fluctuation in the probe deflection indicates an oscillation in the flow speed of the same magnitude as the mean flow. However, the probe deflection never became negative; this indicates that the flow was always in the direction of increasing surface tension, but was fluctuating in magnitude. It was suggested in [2] that since the thermocapillary forces were pulling the surface molecules of the hydrogen-bonded network in one direction, the influence of the surface would extend to a greater depth than would be expected if there were no thermocapillary convection. In the Gibbs model of the interface, this additional energy and that produced by stretching and oscillating of the hydrogen bonds parallel to the interface would be assigned to the surface phase.

A one-to-one relation existed between the vapor-phase pressure and the evaporation flux throughout the range of vapor-phase pressures that were experimentally accessible (Fig. 1). The largest value of the Marangoni number reached was 16 134, and as indicated by the energy analysis, the viscous dissipation at the interface was negligible throughout this range; thus, the condition where a transition to a turbulent interface was expected was never reached. Attempts to further increase the evaporation rate (and Ma) led to spontaneous freezing of the liquid.

ACKNOWLEDGMENTS

This work was supported by the Natural Sciences and Engineering Research Council of Canada and by the Canadian Space Agency.

APPENDIX: THERMAL PROPERTIES OF D_2O

The density of $D_2O(\ell)$ has been reported by Zhelezny [27] and by Kazavchinskii and Kirillin [28]. Their data were used to express the density as a function of temperature:

$$n^L = 1103.68 + 0.343087T - 0.00994309T^2 - 0.0000590035T^3 - 0.0000157854T^4 + 4.30406 \times 10^{-7}T^5 + 7.76413 \times 10^{-9}T^6.$$

The surface tension measurements of D_2O reported by Cooper [29] were used determine the expression

$$\gamma^{LV} = 75.5008 - 0.137153T - 0.000328917T^2 + 4.36994 \times 10^{-7}T^3 - 3.3136 \times 10^{-10}T^4.$$

The expression for the viscosity of $D_2O(\ell)$ was obtained from the data reported by Oppipov [30] and is

$$\eta_L = 0.00238962 - 0.0000903929T + 3.05838 \times 10^{-6}T^2 - 2.97818 \times 10^{-7}T^3 - 2.29563 \times 10^{-8}T^4 - 1.00907 \times 10^{-9}T^5.$$

The thermal conductivities of the liquid, κ^L, and vapor, κ^V, phases of D_2O, each phase at the saturation condition, are given by

$$\kappa^L = 0.558787 + 0.00171402T - 0.00001164 41T^2 + 2.2302 \times 10^{-8}T^3$$

and

$$\kappa^V = 0.0162702 + 0.0000704443T + 1.46086 \times 10^{-7}T^2.$$

These expressions were obtained from the data reported by Tanishita [31].

The enthalpies of the liquid and vapor in the saturation state have been reported by Kazavchinskii and Kirillin [32]. Their data may be expressed in terms of the equations

$$h^V = 2.31533 \times 10^6 + 1531.41T + 10.1418T^2 - 0.224032T^3,$$

$$h^L = -15903 + 4185T - 1.16777 \times 10^{-12}T^2 + 1.71624 \times 10^{-14}T^3.$$

Measurements of the saturation vapor pressure as a function of temperature have been reported by Kraus and Greer [33]. Their results are represented by

$$P_s(T) = 495.339 + 37.641T + 1.40308T^2 + 0.0276009T^3 - 0.000677771T^4 - 0.0000374607T^5 + 2.85093 \times 10^{-7}T^6.$$

[1] C. A. Ward and F. Duan, Phys. Rev. E **69**, 056308 (2004).
[2] F. Duan and C. A. Ward, this issue, Phys. Rev. E **72**, 056302 (2005).
[3] F. Duan, V. K. Badam, F. Durst, and C. A. Ward, preceding paper, Phys. Rev. E **72**, 056303 (2005).
[4] S. Popov, A. Melling, F. Durst, and C. A. Ward, Int. J. Heat Mass Transfer **48**, 2299 (2005).
[5] A. Chai and N. Zhang, Exp. Heat Transfer **11**, 187 (1998).
[6] J. R. Pearson, J. Fluid Mech. **4**, 489 (1958).
[7] J. Willard Gibbs, Trans. Conn. Acad. Arts Sci. **3**, 108 (1876); in *The Scientific Papers of J. Willard Gibbs*, edited by H. A. Bumstead and R. G. Van Name (Dover, New York, 1961), Vol. 1, p. 219.
[8] C. A. Ward and G. Fang, Phys. Rev. E **59**, 429 (1999).
[9] C. A. Ward and D. Stanga, Phys. Rev. E **64**, 051509 (2001).
[10] A. J. McGaughey and C. A. Ward, J. Appl. Phys. **93**, 3619 (2003).
[11] P. Rahimi and C. A. Ward, Int. J. Heat Mass Transfer **47**, 877 (2004).
[12] C. A. Ward, J. Non-Equilib. Thermodyn. **27**, 289 (2002).
[13] C. A. Ward, R. D. Findlay, and M. Rizk, J. Chem. Phys. **76**, 5599 (1983).
[14] C. A. Ward, J. Chem. Phys. **79**, 5605 (1983).
[15] J. A. Elliott, H. Y. Elmoazzen, and L. E. McGann, J. Chem. Phys. **113**, 6573 (2000).
[16] J. A. Elliott and C. A. Ward, J. Chem. Phys. **106**, 5667 (1997).
[17] J. A. Elliott and C. A. Ward, J. Chem. Phys. **106**, 5677 (1997).
[18] M. Torri and J. A. Elliott, J. Chem. Phys. **111**, 1686 (1999).
[19] W. Rudzinski and T. Panczyk, J. Phys. Chem. **104**, 9149 (2000).
[20] T. Panczyk and W. Rudzinski, Appl. Surf. Sci. **233**, 141 (2004).
[21] S. A. Rice and M. G. Sceats, J. Phys. Chem. **85**, 1108 (1981).
[22] A. R. Henn and W. Kauzmann, J. Phys. Chem. **93**, 3770 (1989).
[23] A. R. Henn, Biophys. Chem. **105**, 533 (2003).
[24] J. Hegseth, N. Rashidnia, and A. Chai, Phys. Rev. E **54**, 1640 (1996).
[25] R. Lemus, J. Mol. Spectrosc. **225**, 73 (2004).
[26] L. D. Landau and E. M. Lifschitz, *Fluid Mechanics* (Pergamon, London, 1959).
[27] B. V. Zhelezny, Russ. J. Phys. Chem. **43**, 1311 (1969).
[28] Y. Z. Kazavchinskii and V. A. Kirillin, *Heavy Water—Thermophysical Properties* (Jerusalem Israel Program for Scientific Translations, Jerusalem, 1971).
[29] J. R. Cooper (unpublished).
[30] Y. A. Oppipov, B. V. Zheleznyi, and N. F. Bondarenko, Russ. J. Phys. Chem. **51**, 1311 (1977).
[31] I. Tanishita (unpublished).
[32] Y. Z. Kazavchinskii and V. A. Kirillin, *Heavy Water—Thermophysical Properties* [28].
[33] G. F. Kraus and S. C. Greer, J. Phys. Chem. **88**, 4781 (1984).